Control of the dipole layer of polar organic molecules adsorbed on metal surfaces via different charge-transfer channels

Meng-Kai Lin,[1] Yasuo Nakayama,[2] Ying-Jie Zhuang,[1,3] Kai-Jun Su,[1] Chin-Yung Wang,[1] Tun-Wen Pi,[3] Sebastian Metz,[4] Theodoros A. Papadopoulos,[5*] Tai-Chang Chiang,[3,6] Hisao Ishii,[7,8] and Shu-Jung Tang[1,3#]

1. *Department of Physics and Astronomy, National Tsing Hua University, Hsinchu, Taiwan 30013, Republic of China*

2. *Department of Pure and Applied Chemistry, Tokyo University of Science, 2641 Yamazaki, Noda, Chiba 278-8510, Japan*

3. *National Synchrotron Radiation Research Center (NSRRC), Hsinchu, Taiwan 30076, Republic of China*

4. *Scientific Computing Department, STFC Daresbury Laboratory, Daresbury, Warrington WA4 4AD, U.K.*

5. *Department of Natural Sciences, University of Chester, Thornton Science Park, Chester CH2 4NU, U.K.*

6. *Department of Physics, University of Illinois at Urbana-Champaign, 1110 West Green Street, Urbana, Illinois 61801-3080, U.S.A.*

7. *Graduate School of Advanced Integration Science, Chiba University, 1-33 Yayoi-cho, Inage-ku, Chiba 263-8522, Japan*

8. *Center for Frontier Science, Chiba University, 1-33 Yayoi-cho, Inage-ku 263-8522, Japan*

Abstract

Organic molecules with a permanent electric dipole moment have been widely used as a template for further growth of molecular layers in device structures. Key properties of the resulting organic films such as energy level alignment (ELA), work function, and injection/collection barrier are linked to the magnitude and direction of the dipole moment at the interface. Using angle-resolved photoemission spectroscopy (ARPES), we have systematically investigated the coverage-dependent work function and spectral line shapes of occupied molecular energy states (MES) of chloroaluminium-phthalocyanine (ClAlPc) grown on Ag(111). We demonstrate that the dipole orientation of the first ClAlPc layer can be controlled by adjusting the deposition rate and post annealing conditions; the ELA at the interface differs by ~0.4 eV between the Cl-up and -down configurations of the adsorbed ClAlPc molecules. These observations are rationalized by density-functional-theory (DFT) calculations based on a realistic model of the ClAlPc/Ag(111) interface, which reveal that the different orientations of the ClAlPc dipole layer lead to different charge-transfer channels between the adsorbed ClAlPc and Ag(111) substrate. Our findings provide a useful framework towards method development for ELA tuning.

Introduction

The field of organic electronics and optoelectronics has been rapidly developing as organic materials offer a broad array of functionalities for applications including organic light emitting diodes,[1] organic field effect transistors,[2,3] and organic solar cells.[4] A typical organic device includes at least two organic semiconductor layers and two metal and/or metal oxide electrodes to provide for charge injection/collection, while device performance depends critically on charge transfer at the metal/organic and metal-oxide/organic interfaces.[5-7] Charge transfer determines ELA, which characterizes the energy differences between the electrode Fermi level and the highest occupied molecular orbital (HOMO) and lowest unoccupied molecular orbital (LUMO) in the adjoining organic film. These energy differences give rise to charge injection/collection barriers related to the efficiency of the device.[7] Large efforts have been made to control the ELA, including the incorporation of doping,[8] selection of metal substrates of suitable work functions,[9] tuning of the interfacial

gap states,[10] and employment of a network of donor/acceptor organic layers;[11] the common underlying theme is to modify and thus control charge transfer at the interface. Utilizing polar molecules for interface modification is a particularly powerful approach; the MES associated with a charged atom or functional group of the polar molecule could overlap and thus interact strongly with the substrate states, resulting in substantial charge transfer.

Using spot-profile analysis, low-energy electron diffraction, and X-ray standing wave methods, Stadler *et al.* observed various structural phases of adsorbed tin-phthalocyanine (SnPc) on a Ag substrate, depending on the deposition temperature and molecular coverage.[12] Dependence of the ELA on the polar-molecule orientation and packing density has also been reported[13-22], and connection to device applications has been demonstrated.[23-25] Hosokai *et al.*, who compared the as-grown (AG) and annealed (AN) chlorogallium-phthalocyanine (ClGaPc) films grown on highly oriented pyrolytic graphite (HOPG), reported large band bending of the HOMO state for the AG films with a stacked bilayer structure, but this band bending could be suppressed in the AN films because of the formation of a uniform Cl-up configuration after the thermal treatment;[13] the substrate, HOPG, was however fairly inert in this case, and charge transfer at the organic/metal interface was expected to be minimal. Huang *et al.*[22] investigated the molecular-orientation-dependent electronic properties of a ClAlPc monolayer (ML) on Au(111) and concluded that both Cl-up and -down configurations coexist in AG ML films. They suggested that after annealing, only the Cl-up configuration remains, and this re-orientation was found to be accompanied by a large negative vacuum level (VL) shift.

The focus of the present paper is to investigate how interface charge transfer and molecular orientation of ClAlPc, in the ML region, can be controlled by varying the sample preparation conditions. Smooth thin films of Ag were grown on Ge(111) to serve as substrates for ClAlPc growth. We have analyzed photoemission line shapes of the MES and VL shifts of films with various ClAlPc coverages prepared under different deposition rates before and after annealing. From these results, key factors that determine the orientation of the ClAlPc dipole layer are isolated. In contrast to previous results of ClGaPc on HOPG and ClAlPc on Au(111),[13, 22] we find it feasible to grow a ML of either Cl-up or Cl-down configuration on Ag(111), leading to a significant difference in charge transfer at the interface. Further growth of ClAlPc on top of these two different ML templates reveals considerable differences in ELA, up to ~0.4 eV, demonstrating our ability to control the interfacial molecular configuration and thus the system properties by adjusting the growing conditions.

Experimental and computational details

N-type Ge(111) wafers were chosen as the starting substrate. Standard sputtering and annealing procedures were followed to yield a clean Ge surface exhibiting the c(2×8) reconstruction[26]. Ag films of 7, 9, and 12 ML were then deposited onto the Ge(111) substrate maintained at −140 °C followed by mild annealing to room temperature in order to form smooth Ag(111) films[26]. The Ag films thickness was determined by the energy positions of Ag quantum-well states[26]. We observed that the change in Ag-film thickness in the range studied in our experiment does not affect the results reported below [Fig.S1-S4]. ClAlPc and phthalocyanine (H$_2$Pc or Pc) molecules were then deposited on the Ag films and were maintained at room temperature to form the AG films. The deposition rate and coverage of ClAlPc were determined using a pre-calibrated quartz thickness monitor, according to which the threshold temperature of evaporation is 250 °C. The evaporation temperatures corresponding to ClAlPc deposition rates of 0.1, 3, and 5 Å/min are 275, 315, and 335 °C,

respectively. The AN samples were obtained by raising the temperature to 60 °C slowly after ClAlPc deposition, with the rate of 3 Å/min, and then maintained at that temperature for an hour. Here, 1 ML refers to a close-packed molecular layer with the molecular π plane oriented parallel to the substrate; it is determined by the coverage-dependent VL shift and further calibrated by the photoemission intensity ratio between ClAlPc MES and Ag substrate states. Higher coverages were approximated via a linear relation with the deposition time. ARPES measurements were performed using 50 eV photons and a Scienta R3000 analyzer at beamline 08A1-LSGM of the National Synchrotron Radiation Research Center (NSRRC), Hsinchu, Taiwan. The energy resolution was 50 meV, and the acceptance angle was ±5°. Spectra were taken along the symmetry direction $\bar{\Gamma}\bar{M}$ of the Ag(111) surface Brillouin zone. To determine the VL[7], the sample was electrically biased at −6.0 V at normal emission in order to shift the secondary electron cutoff into an energy range suitable for detection by the electron analyzer. The Fermi level position was extracted from the Fermi edge of the Ag substrate.

In terms of our theoretical methodology, the Vienna Ab Initio Simulation Package (VASP), version 5.3.3[27,28], was employed in order to construct a computational model of the metal/organic interface. The semi-local exchange-correlation functional PW91 under the generalized gradient approximation,[29] was used along with the Grimme DFT-D2 method,[30] in which van der Waals interactions are described via a pair-wise force field. All calculations were performed using plane-wave basis sets, and the projector augmented wave (PAW) method[31,32] with a plane-wave cut-off energy of 400 eV. In addition, a Γ centered k-point grid of 6×6×1 was employed for all calculations related to electronic structure, while geometry optimization of the surface involved a k-point grid of 1×1×1. The Methfessel-Paxton scheme with a width of 0.2 eV was used to determine how partial occupancies are set for each wave function. The Ag(111) substrate was modeled by a five-layer slab, each layer containing 64 Ag atoms within a simple orthorhombic cell of dimensions a = 23.11 Å, b = 20.01 Å and c = 45.00 Å; initial crystal structure and atomic coordinates were taken from the work by Owen et al.[33] Geometry optimization, with maximum residual atomic forces of 0.01 eV·Å^{-1}, was carried out for the top two Ag layers emulating surface relaxation, while the bottom three layers were kept fixed at its crystallographic coordinates representing "bulk" silver.[5] In order to construct the ClAlPc/Ag(111) interface, the ClAlPc molecules were imported on the metal surface with a lateral distance of about 5 Å between nearest-neighbor molecules, equivalent to a surface coverage density of $2.16×10^{13}$ cm^{-2}, to avoid steric effects between them. Such coverage is about ⅓ of the experimentally observed packing density of ~$6.38×10^{13}$ cm^{-2} for ClAlPc molecules adsorbed on the Ag(111) surface.[34] Geometry optimization was re-initiated and both Cl-up and -down configurations were found to bond favorably on a hollow Ag(111) site. For the Cl-down configuration, the atomic distance between Cl and its three Ag nearest neighbors was found to be 2.58 Å on average, while the Al-Cl atomic distance was found to be 2.22 Å for the Cl-down and 2.16 Å for the Cl-up configuration. Illustrations of the structures in this work were constructed using the visualization tool VESTA.[35]

Results and Discussion

I. Adsorption configurations of planar and polar Pc molecules

Figures 1(a) and (b) show schematically the chemical structure of planar H_2Pc and polar ClAlPc, respectively. The main difference between the two molecules is the replacement of the two protons in the middle of H_2Pc with an Al-Cl unit, generating for the latter a permanent dipole moment of 3.7 Debye for a freestanding ClAlPc.[17] It is expected that H_2Pc prefers a flat-lying orientation on the Ag(111) surface to

maximize molecular bonding over a large contact area. For ClAlPc, the Cl atom protrudes out of the molecular plane, leading to two possible adsorption configurations: Cl-up or -down [Fig. 1(c)]. While the former interacts in a similar fashion with the Ag surface as H_2Pc via the delocalized π electron system associated with the ligand, the latter introduces a strong Ag-Cl interaction. In view of the large differences in electronegativity[36] between Cl and Ag, 3.16 vs. 1.93, the Cl-down configuration is expected to involve significantly different charge transfer between the molecule and the substrate, which can be quantified by ARPES as discussed in the following sections.
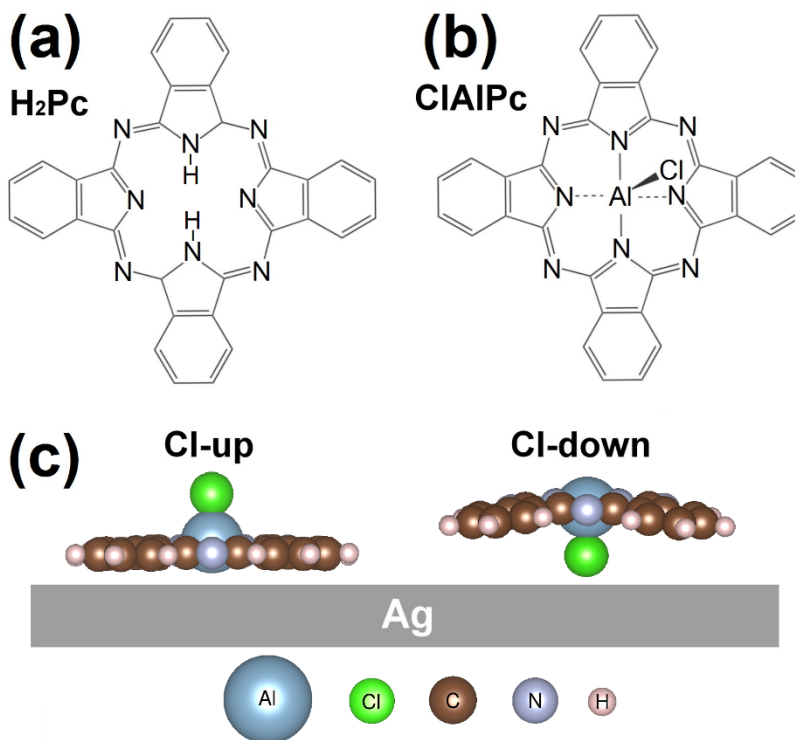

Fig. 1 The chemical structure of (a) H_2Pc and (b) ClAlPc and the corresponding side views of the ClAlPc/Ag(111) interface for the Cl-up and -down configuration (c). The pink, grey, brown, green, and blue spheres represent the H, N, C, Cl, and Al atoms respectively.

II. Coverage-dependent VL shifts

A VL shift from negative to positive values and vice versa is related to changes in orientation of the molecular or interface dipole, as described both experimentally and theoretically for a number of cases discussed in the literature.[37,38] Figure 2(a) shows the coverage-dependent VL shifts for H_2Pc, AN ClAlPc, and AG ClAlPc on Ag(111) prepared by deposition at a 3 Å/min rate, while Figure 2(b) shows the VL shifts of AG ClAlPc prepared at three deposition rates: 0.1, 3 and 5 Å/min. In Fig. 2(a), the VL for H_2Pc descends upon initial deposition and then gradually saturates at about 3-Å coverage. The initial decrease can be attributed to two effects: first, charge transfer from H_2Pc to Ag(111) due to the lower work function of H_2Pc,[10] and second, a push-back effect due to the suppression of the Ag(111) surface dipoles by the adsorption of H_2Pc.[7,39].

As for the adsorption of ClAlPc, in spite of possible slight variations caused by the deposition rate and growing condition, coverage of 3.5 Å is defined as 1 ML, above which VL shifts start exhibiting distinct behaviors over the coverage for AG and AN ClAlPc on Ag(111), i.e. VL shift starts saturating or decaying. A sharp downward shift of VL, about −0.1 eV, upon initial coverage of ~0.3 Å, is common for all cases; it can be attributed to the push-back effect because of the higher ClAlPc work function as compared to that of Ag.[25]

The VL then rises sharply for the AG films at higher coverages beyond 0.3 Å. Interestingly, the AN film shows much smaller variations at higher coverages as explained in the following paragraph. This is in contrast to prior published results for 1-ML ClAlPc films on Au(111),[22] where a large downward VL shift of −0.45 eV was observed for the AG films, while post annealing led to even larger negative VL shifts of −0.89 eV. On the other hand, in the case for AN ClGaPc on HOPG,[13] positive VL shifts at 1 ML were observed and attributed to the ClGaPc electric dipole of the Cl-up configuration. Both ClAlPc on Au(111) and ClGaPc on HOPG[13,22] are known to host Cl-up and -down orientations for the AG films, where the electric dipole contributions from the two orientations mutually cancel.

Since Ag has a lower electronegativity, $\chi_{Ag}=1.93$, than that of Au, $\chi_{Au}=2.4$, we would expect the metal-to-molecule charge transfer for the Ag substrate to be stronger, especially for the Cl-down configuration, thus forming an interface dipole causing possibly a larger VL shift. For reference, a previous theoretical study of adsorption of halogens on Cu(111) has indicated that Cl atoms can increase the VL by over 1 eV at a coverage of 0.5 ML;[40] the larger shift is consistent with the electronegativity difference. Figure 2(b) reveals an interesting trend that the positive VL shifts at higher coverages are larger with a slower deposition rate. In light of the above discussion of how the interfacial dipole moment depends on the molecular orientation, the results imply that a slower deposition rate tends to favor a Cl-down configuration. In the following, we present evidence for this proposal.
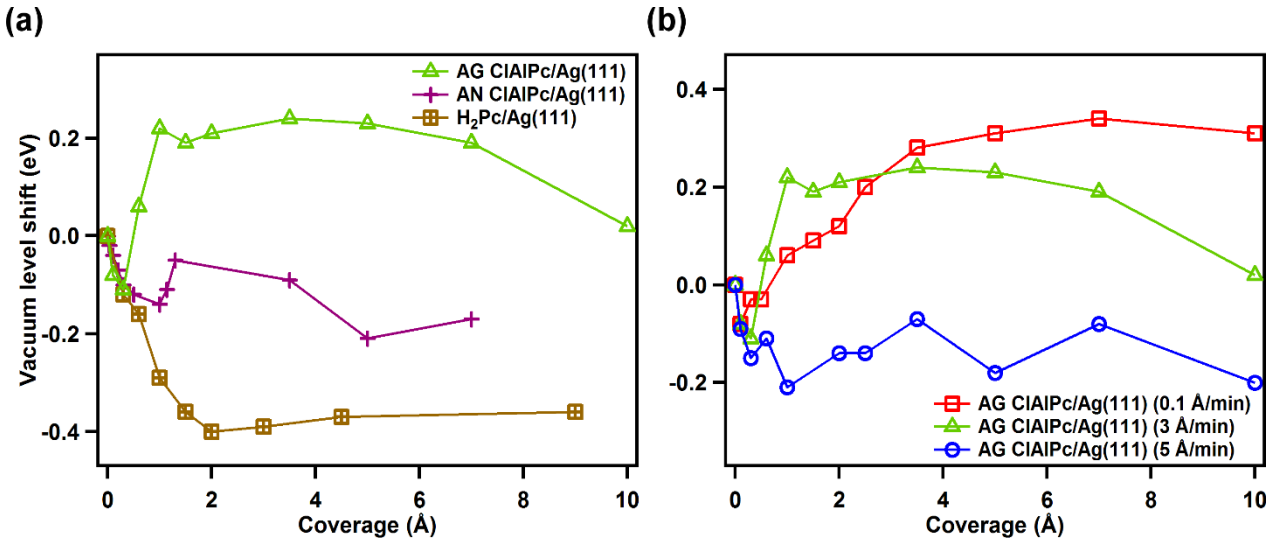

Fig. 2 VL shift as a function of coverage for (a) H_2Pc, AG ClAlPc, and AN ClAlPc on Ag(111), and (b) AG ClAlPc on Ag(111) for various deposition rates, i.e. 0.1 Å/min, 3 Å/min, and 5 Å/min.

III. Coverage-dependent MES spectral line shapes

Figure 3 shows the evolution of photoemission line shapes with increasing coverages for AG ClAlPc with deposition rates of 0.1, 3 and 5 Å/min. The peaks within about 3 eV below the Fermi level are derived from the surface state and quantum-well states of the Ag(111) films;[10] their intensities decay for increasing coverages of ClAlPc. The features between −4 and −8 eV are mostly Ag-derived 4d states. At higher binding energies MES features are observed arising from the adsorbed molecules. Three peaks at about −8.48, −9.71, and −11.4 eV can be identified. Their intensities evolve differently depending on the deposition rate. We observe that for a slow deposition rate, i.e. 0.1 Å/min [Fig. 3(a)], a single MES peak at −9.71 eV dominates along with a minor contribution from a peak at −11.4 eV. For the rapid deposition rate, i.e. 5 Å/min [Fig. 3(c)],

5

we observe that the previously dominant peak at −9.71 eV has now become negligible to a peak at −8.48 eV which dominates the photoemission landscape. In terms of the fast deposition rate at 3 Å/min [Fig. 3(b)], the spectra reveal an intermediate situation, where an almost equal contribution from both MES peaks at −9.71 and −8.48 eV exists. These distinct features observed in the photoemission landscapes of Fig. 3 resemble the dependence of VL shift on coverage and deposition rate [Fig. 2(b)] and further imply the link between molecular adsorption geometry and deposition rate.
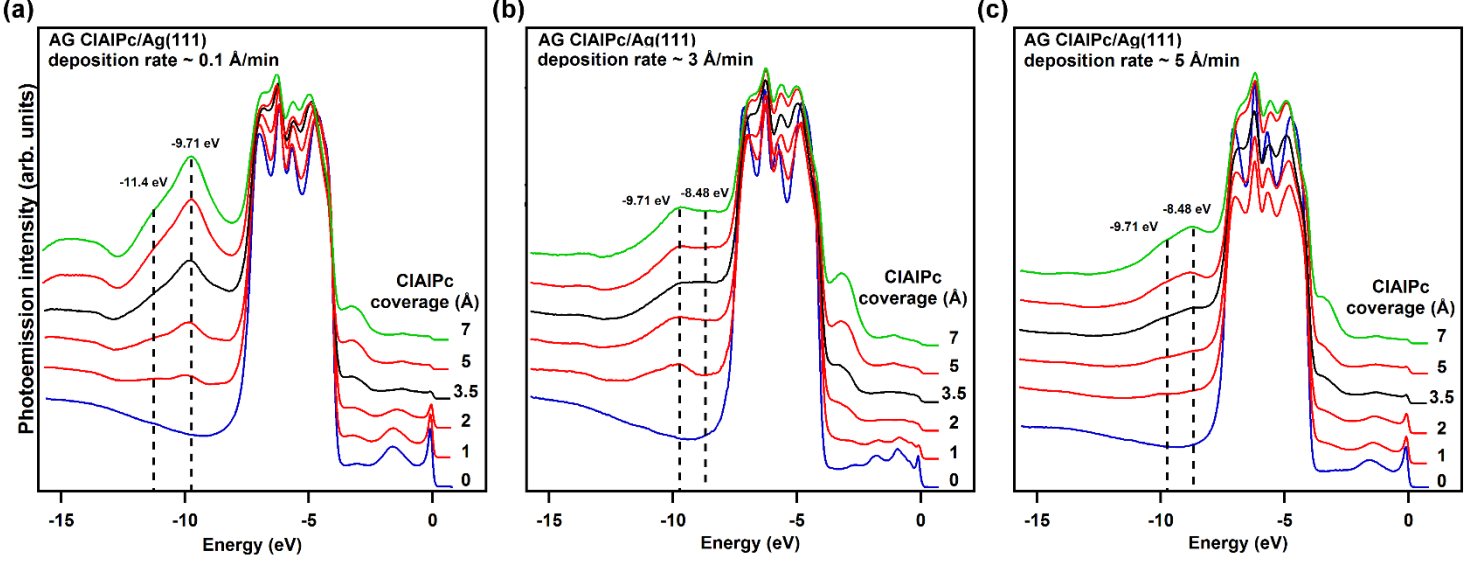

Fig. 3   Coverage dependent angle-resolved photoemission spectra integrated from −0.3 Å⁻¹ to 0.3 Å⁻¹ for AG ClAlPc at a deposition rate of (a) 0.1 Å/min, (b) 3 Å/min, and (c) 5 Å/min. Blue, black and green colors denote the EDCs corresponding to ClAlPc at 0, 1, and 2 ML.

IV. Correspondence between MES spectral line shapes and adsorption configurations

To identify the origins of the MES peaks of Fig. 3, we compare in detail photoemission energy distribution curves (EDCs) taken from 1 ML of H_2Pc and 1 ML of AN ClAlPc [Fig. 4(a)]. A similar comparison is also made for 1 ML of AG ClAlPc prepared at deposition rates of 3 and 0.1 Å/min [Fig. 4(b)]. The line shapes can be well described by Lorentzians on a smooth polynomial background as indicated by the fitting curves in green, brown and grey colors. As evident from Fig. 4(a), the line shapes for H_2Pc and AN ClAlPc are similar, each dominated by a peak at about −8.8 eV. As mentioned in the Results and Discussion section I, H_2Pc lies flat on the Ag substrate. The similarity thus suggests that the dominant adsorption configuration of the AN ClAlPc sample is that of the Cl atom protruding above the Pc plane (Cl-up configuration). The spectra for the AG samples [Fig. 4(b)] show a distinctive component at −9.71 eV, which we identify as a feature derived from a Cl-down configuration. For the sample prepared by fast deposition (3 Å/min), the two components (green and brown curves) show nearly equal intensity, which indicates the co-existence of similar populations for Cl-up and -down configurations [Fig. 4(b), top panel]. For the sample prepared by slow deposition (0.1 Å/min), the component at −9.71 eV dominates, suggesting that the sample consists of mostly Cl-down molecules on the surface [Fig. 4(b), bottom panel].

We observe that the above interpretation is in agreement with the VL shifts shown in Fig. 2(b). For fast deposition (green triangles), the equal populations of the Cl-up and -down configurations lead to no net dipole moment, and so the VL shift saturates after the initial dip caused by pushback. For slow deposition (red

squares), the VL shift at higher coverages (1 ML and beyond) is much larger; the positive shift is consistent with the direction of the interfacial dipole layer for the Cl-down configuration.
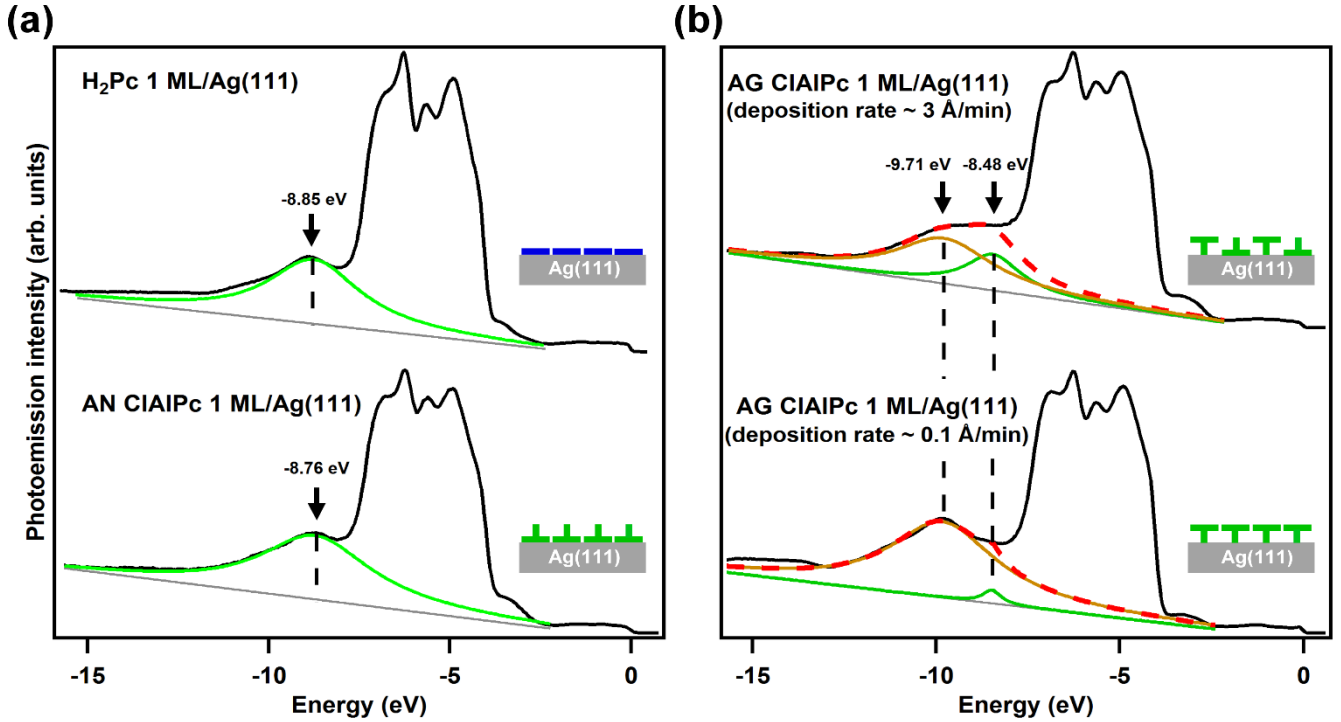

Fig. 4   Angle-resolved photoemission spectra integrated from −0.3 Å^{-1} to 0.3 Å^{-1} for (a) 1-ML H$_2$Pc and 1-ML AN ClAlPc on Ag(111), and (b) 1-ML AG ClAlPc on Ag(111) at the deposition rates of 3 and 0.1 Å/min. The brown and green curves indicate two components from fitting. The gray curve indicates the fitting background. The red dashed curve represents the total fitting curve.

V. Comparison between MES spectral line shapes and calculated DOS

To confirm the relation between the MES line shapes and ClAlPc adsorption configurations, we have constructed a computational model for the Cl-up and -down configurations adsorbed on Ag (111), according to the theoretical procedure described in the methodology section. The middle panel of Fig. 5 shows the calculated total density of states (DOS) of Cl-up and -down ClAlPc as well as the partial DOS projected onto the outer phenylene groups (OPG) and the inner ligand ring (ILR); the ILR is composed of N atoms and inner C atoms that are not part of the phenylene groups. The lower panel of Fig. 5 shows the calculated partial DOS related to the Cl and Al atoms of the ClAlPc adsorbate. An energy shift of −1.3 eV was introduced to the calculated DOS in order to provide an adequate match with the measured photoemission spectra and allow ease of comparison; this is a typical procedure, followed often in the literature,[41] to compensate for the limitations within the approximate implementation of electron exchange and correlation as well as the self-interaction error that play a prominent role in the description of valence states in DFT.[42]

The partial DOS corresponding to the calculated HOMO and LUMO of the adsorbate is located at ~1.2 eV below and ~0.4 eV above the Fermi level (E$_F$ = 0 eV), respectively, for both configurations. While reliable physical interpretation of the energy difference between HOMO and LUMO may be restrictive depending on the DFT approximation used,[43,44] for the ClAlPc/Ag(111) interface studied here, the corresponding energy difference was found to be ~1.6 eV, in mild contrast to the measured value of 1.9 eV reported for the ClAlPc/ITO interface.[45] Although the nature of the two interfaces is different, the calculated HOMO-LUMO

energy difference is not far off the reported experimental value, which provides a clear indication of the reliability of our computational model. The discrepancy of 0.3 eV is related to the well-known limitation of conventional DFT that tends to underestimate the band gap of semiconductors and insulators. Flores et al.[46] have shown that, for organic molecules lying flat on Cu and Ag, conventional DFT predicts interface properties reliably, which justifies our choice to study the ClAlPc/Ag(111) interface via DFT. Finally, our computational model predicts that the work-function of the Ag(111) surface is 4.56 eV (Fig. S10), which is within the experimental values provided in the literature,[47] confirming the validity of our model.
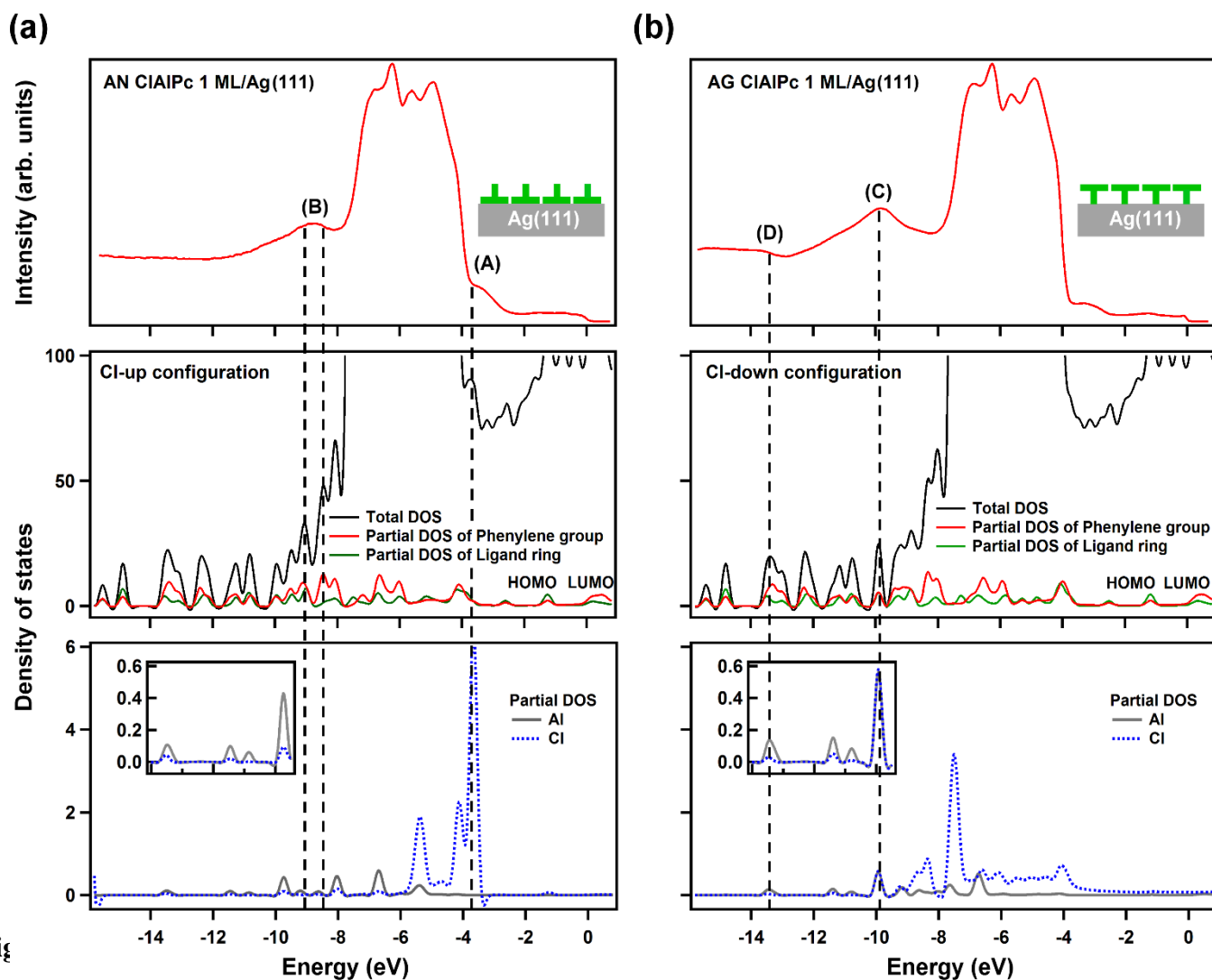

Fig... on Ag(111) and (b) 1-ML AG ClAlPc at the deposition rate of 0.1 A/min (upper panel), together with the calculated total DOS of the ClAlPc/Ag(111) interface and partial DOS of the outer phenylene groups and inner ligand ring (middle panel) as well as the partial DOS of the Cl and Al atoms (lower panel) as a function of energy relative to Fermi level (0 eV) for the Cl-up and Cl-down configuration. An offset of −1.3 eV has been imposed on the computational DOS. The insets show the magnified view for partial DOS of Cl and Al in the energy range from −14 to −9.5 eV.

Because the LUMO lies fairly close to the Fermi level, its tail reaches the Fermi level and imparts an n-type character to the adsorbed molecules. Gap states of this nature near the Fermi level are indeed observed in the photoemission spectra of the AG and AN ClAlPc on Ag(111) films [Fig. S5]. Such charge transfer at the interface would likely modulate the adsorbate DOS causing disparate charge redistribution of the MES

over energy and space due to different charge-transfer channels from Ag(111) at different adsorption configurations.

Figure 5(a) shows, for comparison, the photoemission spectrum of 1-ML AN ClAlPc (upper panel), the calculated total and partial DOS of OPG and IRL (middle panel), and the partial DOS derived from the Al and Cl atoms (lower panel) for the Cl-up configuration. Of interest are two peaks at −3.8 eV (A) and −8.8 eV (B). The former corresponds to the $3p$ energy state of the Cl atom (lower panel, blue dotted curve), while the latter corresponds to contributions from the OPG and to a lesser extend from the ILR. This suggests a charge transfer channel via OPG at the ClAlPc periphery [Fig. S8], in which the delocalized π bonds interact with the Ag substrate causing back donation of charges from the Ag surface to the phthalocyanine.[10] A Bader charge analysis reveals a loss of ~0.04 |e| per Ag atom on average at the molecular periphery close to the phenylene rings, while no charge transfer occurs for the Al and Cl atoms. As expected, the Cl atom on top of the adsorbed molecule does not contribute directly to the bonding to the substrate.

For the Cl-down configuration [Fig. 5(b)], the spectrum exhibits two peaks at −9.7 eV (C) and −13.5 eV (D). Feature (C) corresponds to a sharp total DOS peak with contributions from both the ILR and the OPG, but more importantly, to peaks in the partial DOS associated with the Cl and Al atoms. Upon exanimation of the partial DOS contributions in the bottom panel, it is evident from the inset that both Cl and Al atoms (blue dotted and grey curves) have larger contributions (Cl: 0.56, Al: 0.56) than those of the Cl-up configuration (Cl: 0.09, Al: 0.41). The implication is a charge transfer channel connecting the Ag surface and the molecule via the Al-Cl bond. A Bader charge analysis shows a loss of ~0.09 |e| per Ag atom for the three Ag atoms nearest to Cl, and the Cl releases ~0.15 |e| via charge back-transfer to the Al atom. This suggests a strong charge transfer channel via the Ag-Cl bond [Fig. S9]. The net result is a significant interfacial dipole moment, which accounts for the large positive VL shift seen in Fig. 2(b) for the AG film dominated by the Cl-down configuration. The ILR and OPG DOS contributions to feature (D) at −13.5 eV are also about equal but the larger Al contribution (Al: 0.14) than that of the Cl-up configuration (Al: 0.09), as shown in the inset, also indicates the charge transfer channel via the Al-Cl bond being enhanced to cause the emergence of feature (D). Moreover, the MES feature at −11.4 eV as a shoulder of the spectra, which is more obvious for coverage above 1 ML [Fig. 3(a)], also corresponds to two partial DOS peaks contributed by Al around this energy. As expected, the partial DOS contributed from Cl and Al atoms are at higher binding energies in Cl-down configuration than those in Cl-up configuration due to the strong bonding between Cl and Ag.

VI. Physical mechanisms of adsorption-configuration dependence on deposition rate and post annealing

The above results indicate that a slow deposition rate leads to ClAlPc films with a dominant Cl-down orientation. Film formation generally involves three steps: impingement, diffusion, and nucleation to form islands.[48,49] The lower deposition rate allows more time for the incoming molecules to find an energetically favorable adsorption site for the Cl-down orientation because of the strong interaction between Cl and Ag. This is in agreement with a microscopy study of ClAlPc on Cu(111) by Niu *et al*., who found that the Cl atom of ClAlPc in the Cl-down configuration bonds preferably to hollow sites on Cu(111).[50] The bonding to Ag should be similar, as the electronegativity of Cu, χ_{Cu}=1.90, is nearly the same as that of Ag, χ_{Ag}=1.93. A fast deposition rate involves a large number of molecules coming down onto the surface simultaneously, which can hinder the process for each molecule to settle down to a lower-energy configuration. In the limit of a very high deposition rate, we can expect an equal mixture of both Cl-up and -down configurations. While the above

explanation is the most reasonable based on our data, another possibility should be mentioned: the higher temperature used for evaporating ClAlPc at a higher rate might break the Al-Cl bond.[51] This is likely the case for a deposition rate of 5 Å/min at 335 °C; as seen in Fig. 3(c), the peak at −9.7 eV is weak all the way from the initial deposition in contrast with the cases of deposition at 0.1 and 3 Å/min [Fig. 3(a) and (b)]. It is likely that some of the deposited molecules at the high rate are actually Pc molecules resulting from the decomposition of ClAlPc, which would yield a peak at about 8.4 eV [Fig. 4(a)]. This interpretation is also consistent with the significant differences between the VL shifts for deposition at 3 and 5 Å/min [Fig. 2(b)]. We conclude that in our experiment a deposition rate of 3 Å/min is about the maximum rate without breaking up the molecules in significant numbers.
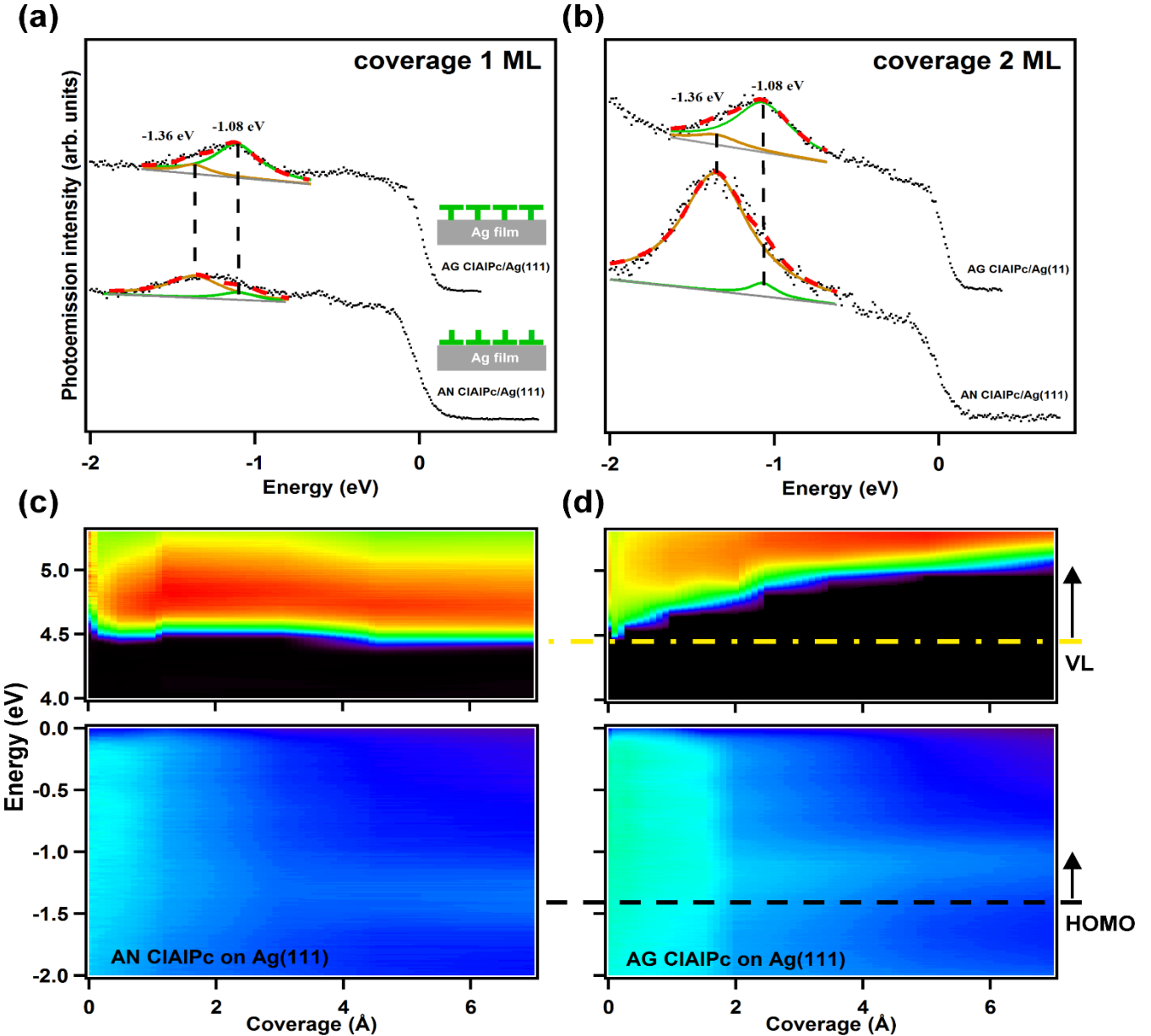

Fig. 6 Angle resolved photoemission spectra at $k_{\parallel} = 0.8$ Å^{-1} for (a) 1-ML AG and AN ClAlPc and (b) 2-ML AG and AN ClAlPc on Ag(111). The brown and green curves indicate two fitting components. The gray curve indicates the fitting background. The red dashed curve represents the total fitting curve. The brown and green curves indicate two fitting components. Also shown are 2-dimensional images of VL and HOMO position as a function of ClAlPc coverage for (c) AN ClAlPc and (d) AG ClAlPc on Ag(111).

Annealing after deposition should allow the film to find a lower energy configuration. According to our

theoretical calculations, the Cl-down and -up configurations correspond to adsorption energies of −3.56 and −5.22 eV, respectively. The energy barrier for conversion from one to the other is likely very high if it involves the flipping of the adsorbed molecules. However, the different behavior in VL shift (Fig. 2) and spectral line shape (Fig. 4 and 5) for the AN films, relative to the AG films, suggest that reorientation of the molecular dipole does occur. One possible low-barrier pathway is for the Cl atom to tunnel through the phthalocyanine molecular plane *via* a process of rotation around the Al atom.[52] We believe that this is the most probable mechanism in our case.

VII. ELA change between adsorption configurations of opposite dipole directions

ELA at the interface is intimately related to the orientation of the dipole layer.[13-22] In Fig. 2, a large increase up to ~0.4 eV in VL is observed for 1-ML AG ClAlPc at the deposition rate of 0.1 Å/min relative to 1-ML AN ClAlPc. If this is related to ELA, the corresponding HOMO positions should change correspondingly. Figure 6(a) shows an off-normal ($k_\parallel = 0.8$ Å^{-1}) photoemission spectrum focusing on the HOMO states of 1-ML AN ClAlPc and AG ClAlPc on Ag films. The data can be described in terms of two peaks at about −1.36 and −1.08 eV (brown and green curves). The −1.36 eV peak dominates for the AN case and the −1.08 eV peak dominates for the AG case. Prior studies of ClAlPc on Au(111)[22] have suggested that the two components of HOMO at lower and higher energies correspond to Cl-up and -down configurations, respectively. This assignment is consistent with our results and interpretation. The trend of different peak intensities persists to 7 Å (~2 ML) [Fig. 6(b)]. Figures 6(c) and (d) display 2-dimensional images of VL and HOMO as a function of energy and coverage for AN ClAlPc and AG ClAlPc, respectively. Effects on ELA are quite evident; VL and HOMO of AG ClAlPc shift upward by about 0.28 and 0.51 eV with respect to those of AN ClAlPc as indicated by the dashed and dash-dotted lines. These shifts at the higher coverage and appear to converge toward a common saturation value that would correspond to the change in the electron and hole injection barriers, a key parameter for optoelectronics applications.

Conclusions

In this work, we present a detailed study of the parameters that control the growth of different configurations of ClAlPc on Ag(111) films. The parameters explored include Ag film thickness, ClAlPc deposition rate, and post-deposition annealing. Photoemission spectroscopy measurements were performed to determine the variations in work function, MES energies and emission intensities. The results reveal that the deposition rate and post-deposition annealing are crucial in determining the interface dipole configuration, while the thickness of the Ag films does not play a significant role in the thickness range investigated. A low deposition rate favors the Cl-down configuration, and post-deposition annealing reverses the dipole orientation to Cl-up. A simple interpretation is that the protruding Cl is naturally attracted to the Ag surface to form an anchoring point if the molecule is allowed ample time to adjust itself to find a local energy minimum at a hollow site on the Ag(111) surface.[47] A dominant Cl-down configuration results in strong charge transfer and interfacial dipole, leading to a substantial upward VL shift. This configuration, obtained only at a low deposition rate, is metastable in view of its higher calculated adsorption energy value relative to the Cl-up configuration. Higher deposition rates lead to a mixed dipole configuration layer. Post annealing of Cl-down ClAlPc results in the Cl-up configuration becoming dominant, which allows an intimate contact of the phthalocyanine molecular plane with the substrate; the flat adsorption geometry allows the π-electrons to bond

with the Ag substrate. The resulting interfacial configuration resembles that for H_2Pc on Ag, which was also examined in the present study to provide supporting evidence. The activation energy for the conversion of the Cl-down to -up configuration requires further investigation, but the process likely involves the tunneling of the Cl atom through the Pc molecular plane.

Our ability to alter the interfacial dipole layer orientation and consequently to tune the ELA is a key finding relevant to the design of devices based on functional polar-organic molecules. Our conclusions are derived primarily from photoemission measurements supported by first-principles calculations. This work is of strong interest to the organic electronics and optoelectronics community.

Acknowledgements

References

1. Y. H. Chen, Y. J. Chang, G. R. Lee, J. H. Chang, I. W. Wu, J. H. Fang, S. H. Hsu, S. W. Liu, C. I. Wu, and T. W. Pi, Org. Electron. **11**, 445 (2010).
2. W. L. Kalb, S. Haas, C. Krellner, T. Mathis, and B. Batlogg, Phys. Rev. B **81**, 155315 (2010).
3. S. Yogev, R. Matsubara, M. Nakamura, U. Zschieschang, H. Klauk, and Y. Rosenwaks, Phys. Rev. Lett. **110**, 036803 (2013).
4. R. A. Street, M. Schoendorf, A. Roy, and J. H. Lee, Phys. Rev. B **81**, 205307 (2010).
5. T. A. Papadopoulos, H. Li, E. –G. Kim, J. Liu, J. A. Cella, C. M. Heller, A. Shu, A. Kahn, A. Duggal, and J. –L. Brédas, Isr. J. Chem. **54**, 779 (2014).
6. T. A. Papadopoulos, J. Meyer, H. Li, Z. Guan, A. Kahn, and J. –L. Brédas, Adv. Funct. Mater. **23**, 6091 (2013).
7. H. Ishii, K. Sugiyama, E. Ito, and K. Seki, Adv. Mater. **11**, 605 (1999).
8. Y. Gao, and L. Yan, Chem. Phys. Lett. **380**, 451 (2003).
9. Y. L. Huang, E. Wruss, D. A. Egger, S. Kera, N. Ueno, W. A. Saidi, T. Bucko, A. T. S. Wee, and E.Zojer, Molecules. **19**, 2969 (2014).
10. M. K. Lin, Y. Nakayama, C. H. Chen, C. Y. Wang, H. –T. Jeng, T. W. Pi, H. Ishii, and S. –J. Tang, Nat. Commun. **4**, 2925 (2013).
11. J. I. Martínez, E. Abad, J. I. Beltrán, F. Flores, and J. Ortega, J. Phys. Chem.**139**, 214706 (2013).
12. C. Stadler, S. Hansen, I. Kröger, C. Kumpf, and E. Umbach, Nat. Phys. **5**, 153 (2009).
13. T. Hosokai, H. Machida, A. Gerlach, S. Kera, F. Schreiber, and N. Ueno, Phys. Rev. B **83**, 195310 (2011).
14. H. Fukagawa, H. Yamane, S. Kera, K. K. Okudaira, and N. Ueno, Phys. Rev. B **73**, 041302 (2006).
15. S. Kera, Y. Yabuuchi, H. Yamane, H. Setoyama, K. K. Okudaira, A. Kahn, and N. Ueno, Phys. Rev. B **70**, 085304 (2004).

16. S. Kera, K. K. Okudaira, Y. Harada, and N. Ueno, Jpn. J. Appl. Phys. **40**, 783 (2001).

17. H. Fukagawa, S. Hosoumi, H. Yamane, S. Kera, and N. Ueno, Phys. Rev. B **83**, 085304 (2011).

18. S. Kera, H. Yamane, H. Honda, H. Fukagawa, K. K. Okudaira, and N. Ueno, Surf. Sci. **566**, 571 (2004).

19. T. Pasinszki, M. Aoki, S. Masuda, Y. Harada, N. Ueno, H. Hoshi, and Y. Maruyama, J. Phys. Chem. **99**, 12858 (1995).

20. T. Niu, J. Zhang, and W. Chen, J. Phys. Chem. C **118**, 4151 (2014).

21. A. Gerlach, T. Hosokai, S. Duhm, S. Kera, O. T. Hofmann, E. Zojer, J. Zegenhagen, and F. Schreiber, Phys. Rev. Lett. **106**, 156102 (2011).

22. Y. L. Huang, W. Chen, F. Bussolotti, T. C. Niu, A. T. S. Wee, N. Ueno, and S. Kera, Phys. Rev. B **87**, 085205 (2013).

23. A. Natan, L. Kronik, H. Haick, and R. T. Tung, Adv. Mater. **19**, 4103 (2007).

24. S. W. Cho, L. F. J. Piper, A. DeMasi, A. R. H. Preston, K. E. Smith, K. V. Chauhan, P. Sullivan, R. A. Hatton, and T. S. Jones, J. Phys. Chem. **114**, 1928 (2010).

25. V. Chauhan, R. Hatton, P. Sullivan, T. Jones, S. W. Cho, L. Piper, A. DeMasi, and K. Smith, J. Mater. Chem. **20**, 1173 (2010).

26. S.-J. Tang, Wen-Kai Chang, Yu-Mei Chiu, Hsin-Yi Chen, Cheng-Maw Cheng, Ku-Ding Tsuei, T. Miller, and T.-C. Chiang, Phys. Rev. B **78**, 245407 (2010).

27. G. Kresse, and J. Furthmüller, Phys. Rev. B **54**, 11169 (1996).

28. G. Kresse, and J. Furthmüller, Comput. Mater. Sci **6**, 15 (1996).

29. J. P. Perdew, J. A. Chevary, S. H. Vosko, K. A. Jackson, M. R. Pederson, D. J. Singh, and C. Fiolhais, Physical Review B **46**, 6671 (1992).

30. S. Grimme, J. Comp. Chem. **27**, 1787 (2006).

31. P. E. Blöchl, Phys. Rev. B **50**, 17953 (1994).

32. G. Kresse, and D. Joubert, Phys. Rev. B **59**, 1758 (1999).

33. E. A. Owen, and E. L. Yates, Philos. Mag. **15**, 472 (1933).

34. Y. L. Huang, Y. Lu, T. C. Niu, H. Huang, S. Kera, N. Ueno, A. T. S. Wee, and W. Chen, Small **8**, 1423 (2012).

35. K. Momma, and F. Izumi, J. Appl. Crystallogr. **44**, 1272 (2011).

36. J. X. Tang, C. S. Lee, and S. T. Lee, Appl. Phys. Lett. **87**, 252110 (2005).

37. G. Heimel, L. Romaner, E. Zojer, and J. L. Bredas, Acc. Chem. Res. **41**, 721 (2008).

38. J. Hwang, A. Wan, and A. Kahn, Mater. Sci. Eng. R **64**, 1 (2009); erratum Phys. Rev. B **48**, 4978(E) (1993).

39. M. K. Lin, Y. Nakayama, C. Y. Wang, J. C. Hsu, C. H. Pan, S. Machida, T. W. Pi, H. Ishii, and S. –J. Tang, Phys. Rev. B **86**, 155453 (2012).

40. T. Roman, and A. Groß, Phys. Rev. Lett. **110**, 156804 (2013).

41. Yasuo Nakayama, Yuki Uragami, Masayuki Yamamoto, Shin'ichi Machida, Hiroumi Kinjo, Kazuhiko Mase, Kaveenga Rasika Koswattage, and Hisao Ishii, Jpn. J. Appl. Phys. **53**, 01AD03 (2014).

42. J. P. Perdew, K. Burke, M. Ernzerhof, Phys. Rev. Lett. **77**, 3865 (1996).

43. Seidl, A. Görling, P. Vogl, J. A. Majewski, and M. Levy, Phys. Rev. B **53**, 3764 (1996).

44. T. Tsuneda and K. Hirao, J. Chem. Phys. **140**, 18A513 (2014).

45. Cho et *al.* J. Phys. Chem. C **114,** 1928 (2010).

46. F. Flores, J. Ortega and H. Vazquez, Phys. Chem. Chem. Phys. **11**, 8658 (2009).

47. V. S. Fomenko, *Handbook of Thermionic Properties: Electronic Work-functions and Richardson Constants of Elements and Compounds*, Plenum Press, New York (1966).

48. J. J. De Yoreo, and P. Vekilov, Rev. Mineral. Geochem. **54**, 57 (2003).

49. F. J. Himpsel, J. E. Ortega, G. J. Mankey, and R. F. Wills, Adv. Phys. **47**, 511 (1998).

50. T. Niu, M. Zhou, J. Zhang, Y. Feng, and W. Chen, J. Phys. Chem. C **117**, 1013 (2013).

51. S. Kuck, M. Prostak, M. Funk, M. Bröring, G. Hoffmann, and R. Wiesendanger, J. Vac. Sci. Technol. A **28**, 795 (2010).

52. J. L. Zhang, J. L. Xu, T. C. Niu, Y. H. Lu, L. Liu, and W. Chen, J. Phys. Chem. C **118**, 1712 (2014).